Mutational Analysis of the Complex of Human RNase Inhibitor and Human Eosinophil-Derived Neurotoxin (RNase 2)†

Daniel P. Teufel,[‡,§,||] Richard Y. T. Kao,[‡,⊥] K. Ravi Acharya,[§] and Robert Shapiro*[,‡,#]

Center for Biochemical and Biophysical Sciences and Medicine and the Department of Pathology, Harvard Medical School, Cambridge, Massachusetts 02139, and the Department of Biology and Biochemistry, University of Bath, Bath BA2 7AY, U.K.

Received September 16, 2002; Revised Manuscript Received December 16, 2002

ABSTRACT: RNase inhibitor (RI) binds diverse proteins in the pancreatic RNase superfamily with extremely high avidity. Previous studies showed that tight binding of RNase A and angiogenin (Ang) is achieved primarily through interactions of hot spot residues in the 434−460 C-terminal segment of RI with the enzymatic active site; Asp435 of RI forms key hydrogen bonds with the catalytic lysine in both complexes, whereas the other contacts are largely distinctive. Here we have investigated the structural basis for recognition of a third ligand, eosinophil-derived neurotoxin (EDN), by single-site and multisite mutagenesis. Surprisingly, Ala replacement of Asp435 decreases affinity for EDN only by 14-fold, as compared to the several hundred-fold decreases with RNase A and Ang, and individual mutations of three other hot spot residues—Tyr434, Tyr437, and Ser460—have essentially no effect. Ala substitutions of nine additional residues, selected by examining a computational model of the RI·EDN complex, also have no marked impact. Overall, the losses in affinity for the single-residue variants examined account for only ∼25% of the free energy of binding for the complex. However, multisite mutagenesis of RI reveals strong superadditivity of mutational effects, indicating that part of this shortfall reflects negative cooperativity. Replacement of Tyr434 together with Asp435 or Tyr437 increases K_i by 540- and 290-fold, respectively. Thus, the C-terminal region of RI again plays an important role in ligand recognition, although probably smaller than for binding RNase A and Ang. Simultaneous substitutions of three neighboring tryptophans (261, 263, and 318) on RI attenuate affinity even more dramatically (by 4900-fold), indicating that the interactions of this RI region also contribute a considerable amount of the binding energy for the EDN complex. These findings highlight the potential importance of cooperativity in protein−protein interactions and the consequent limitations of single-site mutagenesis for assessing interface energetics.

RNase inhibitor (RI)[1] is a 50-kDa cytosolic leucine-rich repeat (LRR) protein that binds the ∼14-kDa members of the mammalian pancreatic RNase superfamily with extraordinary avidity (for reviews, see refs *3*−*5*). The RNase targets of RI normally reside in the extracellular space or are sequestered into organelles, but small amounts may gain entry to the cytosol and would be highly toxic were it not for the presence of this potent inhibitor (*6*, *7*). RI may also regulate the unusual biological activities exhibited by several RNases, including the proangiogenesis factor angiogenin (Ang) (*8*, *9*).

From the standpoint of molecular recognition, the relatively small range of dissociation constants that have been measured for complexes of RI with natural ligands (0.5−200 fM with four nonorthologous RNase types, refs *4* and *10*−*12*) is remarkable. The sequence identities among these RNases are only ∼25−40% (see ref *13*), and only nine accessible residues are completely conserved or conservatively replaced (*1*, *14*−*18*). In principle, the broad specificity of RI might be achieved through a heavy reliance on interactions with these shared residues and common main-chain elements. However, crystallographic and mutational studies on the complexes of RI with bovine pancreatic RNase A and human Ang have revealed that the inhibitor uses largely distinct interactions for tight binding of these proteins (*2*, *19*−*23*). Moreover, the two complexes are characterized by opposite types of cooperativities in the functioning of their various interface components (*22*, *23*).

Despite these differences, some general characteristics of the docking modes for RNase A and Ang are similar. In each case, one lobe of the ligand occupies the central cavity of the RI horseshoe (Figure 1), and another sits atop the upper face of the horseshoe in the C-terminal region, together forming contacts with 12−13 of the 16 LRR units. In both

† This work was supported by the National Institutes of Health (Grant CA88738 to R.S.), the Endowment for Research in Human Biology, Inc. (Boston, MA), and the Medical Research Council, U.K. (Program Grant 9540039 to K.R.A.)

* To whom correspondence should be addressed. Tel.: (617) 621-6132. Fax: (617) 621-6111. E-mail: Robert_Shapiro@hms.harvard.edu.

‡ Center for Biochemical and Biophysical Sciences and Medicine, Harvard Medical School.

§ University of Bath.

|| Present address: Centre for Protein Engineering, Hills Road, Cambridge CB2 2QH, U.K.

⊥ Present address: Department of Microbiology, The University of Hong Kong, Hong Kong.

Department of Pathology, Harvard Medical School.

[1] Abbreviations: RI, RNase inhibitor; LRR, leucine-rich repeat; Ang, angiogenin; hRI, human RNase inhibitor; EDN, eosinophil-derived neurotoxin; 3W, recombinant hRI in which Trp261, Trp263, and Trp318 are replaced by Ala; des(460), recombinant hRI in which Ser460 is deleted; UpA, uridylyl-(3′→5′)adenosine; pRI, porcine RNase inhibitor.

10.1021/bi026852o CCC: $25.00
Published on Web 01/23/2003

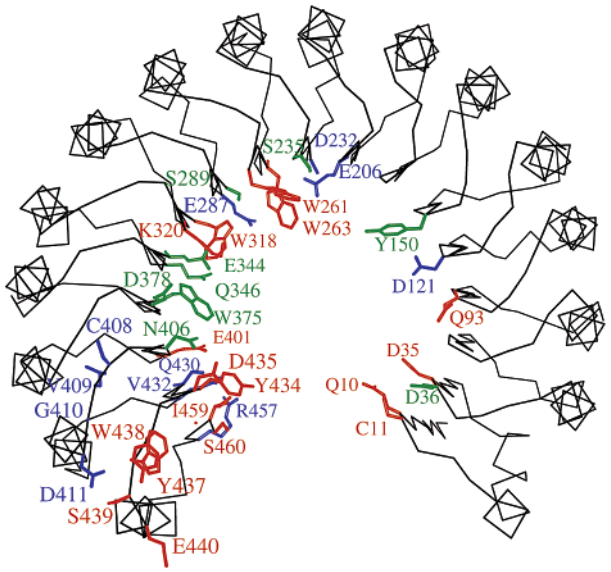

FIGURE 1: Crystal structure of hRI in its complex with Ang (*21*), showing the α-carbon backbone, along with the side chain atoms of residues that contact Ang and/or RNase A [as inferred from the crystal structure of the complex of pRI with RNase A (*19*, *20*)]. Residues that contact only Ang, only RNase A, or both ligands are shown in green, blue, and red, respectively. The figure was drawn with Molscript (*59*).

complexes, the ligand active site makes abundant interactions with the β/α loop 434−440 and Ser460 (human RI (hRI) numbering) that account for a large fraction of the binding energy (*2*, *22*, *23*). Although most of the intermolecular contacts in this region of the two complexes are not the same, one energetically important feature is shared: hydrogen bonds between the catalytic lysine of the ligand (Lys41 of RNase A, Lys40 of Ang) and Asp435 of RI. These observations suggest that the 434−460 region of RI may be a universal hot spot (*24*) for binding all ligands, with the interactions of Asp435 and the fully conserved catalytic Lys serving as a key anchoring point and contacts with more variable active site residues providing much of the additional binding energy (*21*, *23*). The remainder would then derive from largely unique interactions of residues lining the RI cavity outside this region with nonactive-site ligand components.

Here we have performed a mutational analysis of the complex of hRI with a third ligand, human eosinophil-derived neurotoxin (EDN) ($K_i \sim 1$ fM, ref *11*). EDN, also known as RNase 2, is a major component of eosinophil granules (*25*) and is distributed widely in human body fluids and tissues (*11*, *26*−*28*). Our study was undertaken in part to test the mechanistic hypothesis for RI's broad specificity outlined in the preceding paragraph but also to aid in the design of Ang- and EDN-specific derivatives of hRI for use as anticancer agents (*8*, *29*) and as drugs for treatment of hypereosinophilic syndromes (*30*), respectively. Surprisingly, Ala replacement of hRI Asp435 was found to produce only a modest decrease in affinity, and other single-residue changes in the C-terminal segment of RI that dramatically impaired binding of RNase A and/or Ang had little effect. Individual replacements of nine residues outside this region, selected by examining a computational model of the hRI_EDN complex, also failed to influence affinity appreciably. However, substantial losses in avidity were observed when various combinations of hRI residues were replaced. These findings indicate that the C-terminal region of hRI is again important for ligand recognition, although its interactions with EDN are clearly different from those with RNase A and Ang. The effects of multisite mutagenesis also identify a Trp-rich region at the 10−12 o'clock position of the RI horseshoe as a major contributor to binding affinity.

EXPERIMENTAL PROCEDURES

Materials. Human Ang, wild-type hRI, and the hRI variants W261A, W263A, W318A, W261A/W263A/W318A (3W), K320A, Y434A, D435A, Y437A, Y434A/D435A, Y434A/Y437A, and des(460) were produced in *Escherichia coli* as described previously (*2*, *22*, *31*, *32*). Human EDN was purified from urine (*33*). The RNase substrate 6-FAM∼mAmArCmAmA∼Dabcyl was obtained from Integrated DNA Technologies (Coralville, IA) (6-FAM is 6-carboxyfluorescein, mA is 2′-*O*-methyl-riboadenosine, rC is ribocytidine, and Dabcyl is 4-(4-dimethylaminophenylazo)benzoic acid). Sources of other materials and procedures for quantification of Ang, RNase A, and hRI are described by Chen and Shapiro (*22*) or in the references therein. EDN stocks were quantified by titration with hRI in an assay measuring the initial rate of cleavage of UpA (see below) (*34*).

Site-Directed Mutagenesis and Production of Variant Proteins. Fragments of hRI cDNA containing the desired mutations were generated by overlap extension PCR (*35*) as described (*23*). The final PCR products were digested with StuI and either BstX I (R63A and D121A) or EcoR I (S405A, D411A, and E443A) and ligated into pTRP−PRI that had been cleaved by the same enzymes. Sequencing confirmed the presence of the intended mutation and the absence of any spurious changes. Variant proteins were produced in *E. coli*, purified to homogeneity (as judged by SDS−PAGE), and stored as described previously (*32*).

Kinetics. *(A) Assays.* All kinetic experiments were performed in 0.1 M Mes-NaOH (pH 6.0) containing 0.1 M NaCl at 25 °C. This buffer was passed through a C18 Sep-Pak cartridge (Waters) and a 0.45 μ filter to remove adventitious RNases and insoluble materials and was degassed immediately prior to use. Assay mixtures were supplemented with 10 μg/mL of BSA, and incubation mixtures for dissociation measurements were supplemented with 100 μg/mL BSA and 1 mM EDTA. RNase A, EDN, and inhibitor stocks were diluted in water containing 100 μg/mL BSA; inhibitor dilutions also contained 5 mM DTT and 0.1−1 mM EDTA.

(B) Dissociation Rate Constants. Rate constants for dissociation (k_d values) of EDN·inhibitor complexes were determined by a modification of published procedures (*5*, *10*, *11*). In this method, a scavenger for free inhibitor is added to the complex, and the appearance of free EDN is followed by assaying for enzymatic activity. The initial mixture of EDN (100 nM) and inhibitor (150−200 nM) was incubated for 20 min at 25 °C prior to addition of scavenger (Ang, 5 μM final concentration). For some variants, additional incubations were performed as described below. Aliquots (50 μL) were taken periodically for up to 9 days and assayed for activity toward UpA (100 μM); initial velocities were measured spectrophotometrically. The activity of Ang in this assay is undetectable. Control incubations showed that free

EDN retains full RNase activity for >14 days and that no significant amount of EDN is released from the complex in the absence of scavenger for at least 9 days.

As was observed previously for other RI complexes (*2*, *10*, *11*), dissociation was biphasic, with release of 10−23% of the ligand during the first several minutes, followed by a much slower dissociation of the remainder. This biphasic process may reflect heterogeneity in the inhibitor, the ligand, or both (*11*); for example, it is possible that the inhibitor preparations contained some partially oxidized protein with decreased affinity for the ligand. Data for the slower phase (9−14 points per complex) were fitted to a single-exponential decay process with SigmaPlot 2000 (SPSS). For wild-type hRI and all variants except for Y434A and D435A, the 50-fold molar excess of Ang over EDN in the standard dissociation experiments was judged to be adequate to capture essentially all of the free inhibitor: wild-type hRI binds Ang severalfold more tightly than EDN; variants W261A, W263A, W318A, K320A, Y437A, and des(460) were demonstrated previously to retain extremely high affinity for Ang (*2*, *23*); the new variants involve replacements of residues outside the hRI·Ang interface (*21*). Replacements of Tyr434 and Asp435 by Ala increase K_i values for Ang by 250−350-fold (*2*) and have much smaller effects on binding of EDN. Therefore, k_d values for Y434A− and D435A−hRI were calculated from additional data collected with a higher molar excesses of Ang; for Y434A, the concentrations of EDN and inhibitor were reduced by 5-fold and that of Ang was increased by 2-fold, whereas for D435A, the EDN and inhibitor concentrations were decreased by 3.3-fold, and Ang was unchanged.

(C) Association Rate Constants. Rate constants for complex association were determined by monitoring the onset of inhibition in an assay that measures EDN-catalyzed cleavage of the fluorogenic substrate 6-FAM∼mAmArCmAmA∼Dabcyl (*36*, *37*). Assay mixtures contained 100 nM substrate, 3 pM EDN, and 80 pM inhibitor except where noted otherwise; the cleavage reaction was initiated by addition of enzyme and was monitored with a Jobin Yvon-Spex FluoroMax-2 fluorimeter (λ_{ex} = 495 nm, λ_{em} = 525 nm). Under the conditions used, <5% of the substrate was consumed, thereby ensuring that decreases in the rate of cleavage solely reflect loss of free EDN as inhibitor binds. Because of the large molar excess of inhibitor over EDN, the concentration of free inhibitor, [I], did not change significantly during the assay, and association could be treated as a first-order process. Control assays revealed that the complete cleavage reaction (with 100 pM EDN) in the absence of inhibitor is first-order, indicating that the substrate concentration used is well below K_m. In all cases except for the assays with 3W-hRI, association resulted in >99% inhibition, and the apparent second-order rate constant for association, k_a, was calculated as k_{obs}/[I], where k_{obs} is the rate constant obtained by fitting the progress curve to the equation $F_t = F_0 + c(1 - e^{-k_{obs}t})$; F_0 and F_t are the fluorescence values measured at time zero and time t, respectively, and c is an instrument and substrate-related constant. For 3W, the progress curve was fitted to the equation $F_t = F_0 + v_s t + (v_i - v_s)(1 - e^{-k_{obs}t})/k_{obs}$, where v_i and v_s are the reaction velocities (ΔF per second) at the beginning of the assay and after association is complete, respectively. This equation is adapted from that of Cha (*38*). Fits were performed with SigmaPlot 2000. Each k_{obs} value for the multi-residue variants was measured in duplicate, and values for all other variants were measured at least in triplicate. The dependence of k_{obs} on [I] for wild-type hRI was linear at the concentrations used, indicating that k_a represents the true second-order rate constant for association if complex formation occurs in a single step, or that it corresponds to k_2/K_1 if binding follows a two-step mechanism as with Ang and RNase A (K_1 is the equilibrium constant for the initial loose complex EI, and k_2 is the rate constant for conversion of EI to the final tight complex) (*34*, *39*). With D435A-, Y434A/D435A-, and Y434A/Y437A-hRI, which bind less rapidly than wild-type hRI, [I] was increased to 160, 200, and 100 pM, respectively. With K320A-hRI, which binds faster than wild-type hRI, the EDN concentration was doubled to increase the magnitude of fluorescence change.

(D) K_i Values and Binding Free Energies. All inhibition constants except for those of the 3W, Y434A/D435A, and Y434A/Y437A complexes were calculated from k_d and k_a ($K_i = k_d/k_a$); this method is valid for both the single-step and the two-step association mechanisms described above. The K_i values for the multi-residue variants were determined fluorimetrically from the dependence of initial velocity v_0 on [I] as described previously (*23*). The EDN concentrations were 3 pM (3W) or 2 pM (Y434A/D435A and Y434A/Y437A), and substrate was 100 nM.

ΔG values for complex formation were calculated as $-RT \ln K_i$, and changes in binding free energy ($\Delta\Delta G$) associated with amino acid substitutions were calculated as $-RT \ln(K_{i,wt}/K_{i,var})$, where wt and var refer to wild-type and variant hRI. $\Delta\Delta\Delta G$ values for multiple-residue variants are the sum of $\Delta\Delta G$ values for the single-residue variants minus the $\Delta\Delta G$ value measured for the multiple-residue variant. Standard errors were calculated as described previously (*22*).

Modeling of RI·EDN Complex Structures. The 1.6 Å-resolution crystal structure of EDN (PDB code 1HI2, ref *17*) was superimposed onto RNase A and Ang in the crystal structures of the complexes of porcine RI (pRI) with RNase A and hRI with Ang (PDB codes 2BNH, ref *20* and 1B1I, ref *21*, respectively) with the program SHP (*40*). These initial models were subjected to energy minimization by two different methods, both implemented with the program CNS (*41*): (i) conjugate gradient minimization (200 cycles) with no experimental energy terms and (ii) simulated annealing/molecular dynamics as described by Rice and Brünger (*42*). The models obtained by the two procedures did not differ appreciably. An hRI·EDN model described previously (*21*), which was generated with a different program using an earlier EDN crystal structure, is similar to those generated here.

RESULTS

Interactions of Y434A−, D435A−, Y437A−, and des(460)−hRI with EDN. Earlier studies showed that individual replacements of hRI Tyr434, Asp435, and Tyr437 by Ala and deletion of the hRI C-terminal residue Ser460 substantially decrease affinity for RNase A, and in two cases (Tyr434 and Asp435), for Ang as well (*2*, *22*). Therefore, we began our analysis of the hRI·EDN complex by measuring the effects of these mutations on affinity for EDN. The K_i value for the complex of wild-type hRI with EDN from human

Table 1: Kinetic Constants for the Complexes of EDN with hRI Variants Y434A, D435A, Y437A, and Des(460)[a]

hRI	k_d ($s^{-1} \times 10^{-7}$)	$t_{1/2}$[b] (days)	k_a ($M^{-1} s^{-1} \times 10^8$)	K_i (fM)	$K_{i,var}/K_{i,wt}$[c]	$\Delta\Delta G_{EDN}$[d] (kcal/mol)	$\Delta\Delta G_{RNase\ A}$[e] (kcal/mol)	$\Delta\Delta G_{Ang}$[f] (kcal/mol)
wild type	4.0 ± 0.6	20.1	1.48 ± 0.02	2.7 ± 0.4				
Y434A	7.6 ± 0.6	10.6	1.55 ± 0.02	4.9 ± 0.4	1.8	0.4 ± 0.1	5.9	3.3
D435A	16 ± 2	5.0	0.44 ± 0.01	36 ± 5	14	1.5 ± 0.1	3.6	3.5
Y437A	4.6 ± 0.7	17.6	1.36 ± 0.01	3.4 ± 0.5	1.3	0.1 ± 0.1	2.6	0.8
des(460)	3.7 ± 0.4	21.9	1.20 ± 0.03	3.1 ± 0.4	1.1	0.1 ± 0.1	3.5	1.3

[a] Kinetic parameters were measured as described in Experimental Procedures. [b] Half-life for dissociation of the complex. [c] K_i for variant RI divided by that for wild-type RI. [d] $\Delta\Delta G$ values are the difference in binding free energies for the wild-type and variant complexes, calculated from the equation $\Delta\Delta G = -RT \ln(K_{i,wt}/K_{i,var})$. [e] $\Delta\Delta G$ measured for complex of hRI variant with RNase A (*2*). [f] $\Delta\Delta G$ measured for complex of hRI variant with Ang (*2*).

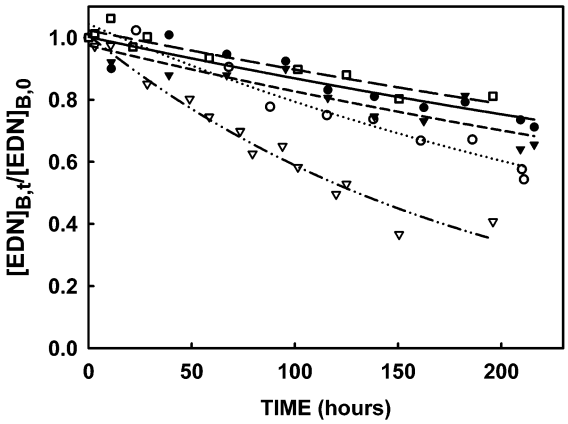

FIGURE 2: Dissociation of the complexes of EDN with hRI variants Y434A, D435A, Y437A, and des(460). Data are plotted as $[EDN]_{B,t}/[EDN]_{B,0}$ vs time for wild-type and variant hRIs, where $[EDN]_{B,t}$ and $[EDN]_{B,0}$ are the concentrations of bound EDN at time t and at the first time point (~5 min), respectively. The lines drawn are the best fits of the data to a single-exponential decay: (from top to bottom) des(460) (open square, long dashes), wild type (filled circle, continuous), Y437A (filled triangle, short dashes), Y434A (open circle, dots), and D435A (open triangle, dash−dot−dot). As noted in Experimental Procedures, the dissociation of all complexes was biphasic, and some EDN was released prior to the initial time point: 10% for wild-type RI and 12, 22, 14, and 22% for Y434A, D435A, Y437A, and des(460), respectively.

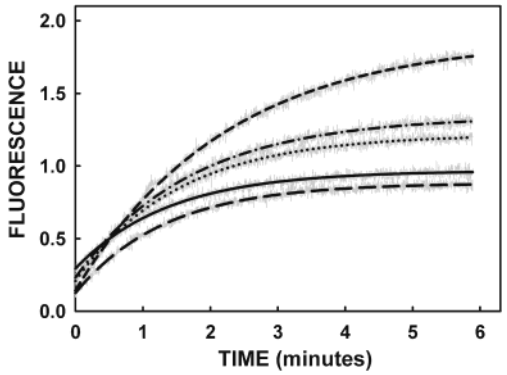

FIGURE 3: Association of the complexes of EDN with hRI variants Y434A, D435A, Y437A, and des(460).The plots show initial rate assays for EDN-catalyzed cleavage of the fluorogenic substrate 6-FAM-mAmArCmAmA-Dabcyl in the presence of wild type and variant hRIs, with the reaction initiated by addition of EDN to a mixture of substrate and inhibitor. The lines drawn are the best fits of the data to a single-exponential rise to maximum: D435A (short dashes), des(460) (dash−dot−dash), Y437A (dots), wild-type (continuous), and Y434A (long dashes).

placenta was determined previously to be 0.9 fM (*11*); this value was calculated from the individual rate constants for dissociation and association. Here we have used a similar approach, except that an improved method for measuring k_a values has been developed. As before, complex dissociation was monitored by the appearance of free EDN after addition of a scavenger for free inhibitor (Figure 2). Values for k_a were obtained directly from the rate of onset of inhibition of EDN's RNase activity at extremely low enzyme and inhibitor concentrations (Figure 3) rather than indirectly as in the earlier study. The k_d and k_a values measured for the wild-type complex were 4.0×10^{-7} s^{-1} and 1.5×10^8 M^{-1} s^{-1}, respectively, yielding a K_i value of 2.7 fM. The ~3-fold difference between this value and that reported earlier may stem from minor changes in incubation conditions or from differences in the N-glycosylation state (*43*) of the urine EDN used here and EDN from placenta.

All four of the mutations in the C-terminal region of hRI had a much smaller impact on binding of EDN than on that of RNase A and Ang (Table 1). The largest increase in K_i, measured for the D435A complex, was 14-fold, reflecting a 4-fold more rapid dissociation (Figure 2) and a 3.4-fold slower association (Figure 3). The corresponding K_i increases for the complexes with RNase A and Ang were 470- and 360-fold, respectively. The K_i value for the Y434A complex was only 1.8-fold higher than with wild-type EDN, as compared to the 23 000- and 250-fold increases observed for the RNase A and Ang complexes. Replacement of Tyr437 by Ala and deletion of Ser460 produced no significant changes in affinity for EDN.

Modeling of the RI·EDN Complex. The complex of RI with EDN was modeled to investigate the structural basis for the effects of the 434, 435, 437, and 460 mutations, as well as to identify other potential interface residues on RI for study. Initial models were generated by superimposing the crystal structure of EDN onto those of Ang in the hRI·Ang complex and RNase A in the pRI·RNase A complex. Both structures were used as targets for superposition because the RI backbones in the two complexes do not align well (*21*). The backbone differences, which reflect the larger opening of the RI horseshoe in the RNase A complex, appear to be dictated by the ligand, and we cannot predict which (if either) structure corresponds to that adopted when EDN is bound. The particular species of RI used in these complexes is probably not an important consideration: hRI and pRI share 77% sequence identity (*44*, *45*), including nearly all residues that contact Ang or RNase A (*20*, *21*), and their affinities for RNase A are indistinguishable (*10*, *39*).

In both superimposition models, well over half of the intermolecular contacts involve the 434−460 segment of RI.

Table 2: Kinetic Constants for the Complexes of EDN with hRI Variants Containing Replacements Outside the 434−437/460 Region[a]

hRI	k_d ($s^{-1} \times 10^{-7}$)	$t_{1/2}$[b] (days)	k_a ($M^{-1}\,s^{-1} \times 10^8$)	K_i (fM)	$K_{i,var}/K_{i,wt}$[c]	$\Delta\Delta G$[d] (kcal/mol)
wild type	4.0 ± 0.6	20.1	1.48 ± 0.02	2.7 ± 0.4		
R63A	2.5 ± 0.4	32.6	1.59 ± 0.02	1.6 ± 0.3	0.6	−0.3 ± 0.1
D121A	3.3 ± 0.5	24.3	1.19 ± 0.02	2.8 ± 0.5	1.0	0.0 ± 0.1
W261A	4.6 ± 0.4	17.3	1.23 ± 0.02	3.8 ± 0.4	1.4	0.2 ± 0.1
W263A	14.1 ± 0.6	5.7	1.22 ± 0.04	12 ± 1	4.3	0.9 ± 0.1
W318A	43 ± 1	1.9	1.33 ± 0.02	32 ± 1	12.0	1.5 ± 0.1
K320A	3.1 ± 0.4	25.5	2.70 ± 0.06	1.2 ± 0.1	0.4	−0.5 ± 0.1
S405A	2.9 ± 0.5	28.0	2.00 ± 0.11	1.4 ± 0.2	0.5	−0.4 ± 0.1
D411A	2.1 ± 0.3	38.0	0.96 ± 0.02	2.2 ± 0.3	0.8	−0.1 ± 0.1
E443A	2.5 ± 0.4	31.7	0.85 ± 0.01	3.0 ± 0.4	1.1	0.1 ± 0.1

[a] Kinetic parameters were determined as described in Experimental Procedures. [b] Half-life for dissociation of the complex. [c] K_i for variant RI divided by that for wild-type RI. [d] $\Delta\Delta G$ values are the difference in binding free energies for the wild-type and variant complexes, calculated from the equation $\Delta\Delta G = -RT \ln(K_{i,wt}/K_{i,var})$.

Asp435 of RI is positioned to hydrogen bond with the catalytic lysine (Lys38). Residues Tyr434, Tyr437, and Ser460 are also close to EDN, and many of the side-chain atoms in fact clash in one or both of the models: Tyr434 with Gln34 and Arg36, Tyr437 with Arg68 and His129, and Ser460 with the N-terminal two residues. When these models were subjected to energy minimization, the conflicts were alleviated by the repositioning of both the RI and the EDN residues involved; in some instances the movements were large. After these rearrangements, RI Tyr434, Tyr437, and Ser460 all remain within contact distance of EDN. Interestingly, the interaction of RI Asp435 with Lys38 of EDN is lost upon energy minimization.

Four additional residues from the C-terminal segment of RI—Val432, Trp438, Glu443, and Ile459—form contacts with EDN in the models. Of these, Glu443 forms the interactions that would seem most likely to contribute significant binding energy: hydrogen bonds with N^{ζ} of Lys1 and $N^{\epsilon 1}$ of Trp7. Outside this region, the 88−95 loop of EDN forms numerous van der Waals contacts with Trps 261, 263, and 318, and a neighboring residue, Lys320, lies within hydrogen bonding distance from Asn39. Several hydrogen bonds outside the C-terminal and Trp-rich regions were also noted, including: (i) three between the side chain of RI Arg63 and EDN residues Gln28, Ser94 and Asn95; (ii) one between RI Asp121 and EDN Arg97; (iii) one between RI Ser405 and EDN Arg36; and (iv) one between RI Asp411 and EDN Arg68.

Effects of Single-Residue hRI Substitutions Outside the 434−437/460 Region. The roles of hRI residues Arg63, Asp121, Trp261, Trp263, Trp318, Lys320, Ser405, Asp411, and Glu443 (Figure 4), all of which feature prominently in the interface in the RI·EDN model complexes, were investigated by single-site mutagenesis. The largest changes were measured with W263A and W318A (4- and 12-fold increases in K_i, respectively); the primary effect in both cases was on k_d (Figure 5, Table 2). None of the other replacements increased K_i significantly, and some (Arg63, Lys320, and Ser405 to Ala) even resulted in tighter binding. For R63A, this improvement reflects primarily slower dissociation, whereas for the other two both k_d and k_a were affected. Dissociation of the D411A and E443A complexes was also somewhat slower than for wild-type, but in these instances association was also slower, so that there was no net effect on K_i.

Interactions of Multi-Residue hRI Variants with EDN. For the hRI·Ang complex, the losses in affinity for multi-residue variants were often more dramatic than would be anticipated if the residues replaced function independently (i.e., the energetic effects of the mutations were superadditive, refs *22* and *23*). The possibility that this might also be the case for the EDN complex was investigated with the hRI Y434A/D435A, Y434/Y437A, and W261A/W263A/W318A (3W) variants.

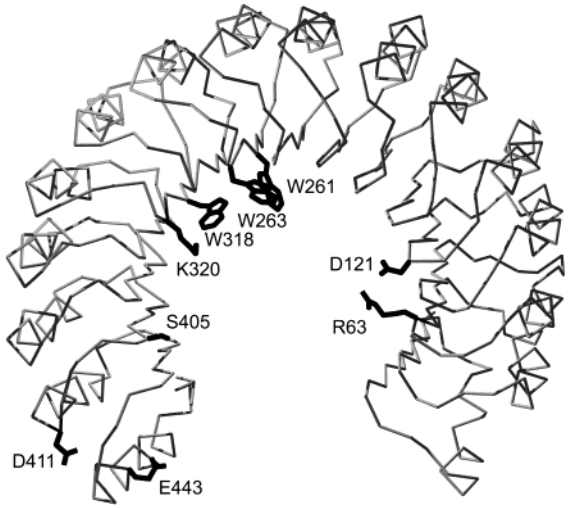

FIGURE 4: Positions of hRI residues selected for mutational study based on modeling. The α-carbon backbone of hRI in its complex with Ang (*21*) is shown, along with the side chains of putative contact residues outside the 434−437/460 region in the modeled RI·EDN complex. The figure was drawn with Swiss-Pdb Viewer and POVRAY (http://www.povray.org).

The method we used to measure K_i values for single-residue variants seemed unlikely to be successful for Y434A/D435A and Y434A/Y437A because Ang binds these variants much less tightly than wild-type hRI (by 100 000- and 74 000-fold, respectively) and would probably be an ineffective scavenger for the dissociation experiments. Therefore, we tested the possibility that the K_i values for these EDN complexes might be high enough so that they could be determined directly from the dependence of v_0 on [I]. For this method to yield accurate K_i values, the amount of time EDN and inhibitor are preincubated prior to addition of substrate must be sufficient for complex association to approach completion. Measurements of the k_a values for Y434A/D435A and Y434A/Y437A (Table 3) indicated that 2 h preincubations would be adequate for initial tests with [I] = 10 pM. Inhibition in these assays was incomplete for both variants, despite the 5-fold molar excess of inhibitor over EDN, suggesting that determination of K_i values by this

Table 3: Kinetic Constants for Complexes of EDN with Multi-Residue hRI Variants[a]

hRI	k_d[b] ($s^{-1} \times 10^{-5}$)	k_a ($M^{-1} s^{-1} \times 10^8$)	K_i (pM)	$K_{i,var}/K_{i,wt}$[c]	$\Delta\Delta G$[d] (kcal/mol)	$\Delta\Delta\Delta G$[e] (kcal/mol)
3W	143 ± 12	1.06 ± 0.06	13 ± 1	4900	5.0 ± 0.1	−2.5 ± 0.2
Y434A/D435A	6.1 ± 1.3	0.42 ± 0.1	1.5 ± 0.3	540	3.7 ± 0.2	−1.8 ± 0.2
Y434A/Y437A	5.8 ± 2.0	0.73 ± 0.03	0.8 ± 0.3	290	3.3 ± 0.2	−2.8 ± 0.2

[a] Kinetic parameters were determined as described in Experimental Procedures. [b] Calculated from the measured values for k_a and K_i. [c] K_i for variant RI divided by that for wild-type RI. [d] $\Delta\Delta G$ values are the difference in binding free energies for the wild-type and variant complexes, calculated from the equation $\Delta\Delta G = -RT \ln(K_{i,wt}/K_{i,var})$. [e] $\Delta\Delta\Delta G$ values are the sum of $\Delta\Delta G$ values for single-residue variants (from Tables 1 and 2) minus the $\Delta\Delta G$ value for the multi-residue variant.

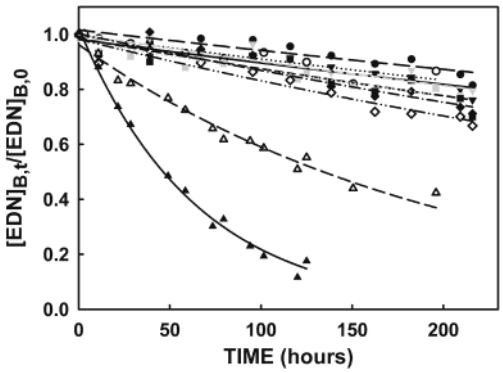

FIGURE 5: Dissociation of complexes of EDN with (listed from top to bottom, black symbols and lines unless indicated otherwise) D411A (filled circles, long dashes), R63A (open circles, dots), E443A (filled triangles, continuous), S405A (gray filled triangles, continuous gray), D121A (filled squares, short dashes), K320A (gray filled squares, gray dots), wild-type hRI (filled diamonds, dash−dot), W261A (open diamonds, dash−dot−dot), W263A (open inverted triangles, short dashes), and W318A (filled inverted triangles, continuous), plotted as in Figure 2. The extents of complex dissociation prior to the initial time point were 10, 16, 17, 12, 13, 13, 16, 12, 17, and 23%, respectively (see Experimental Procedures).

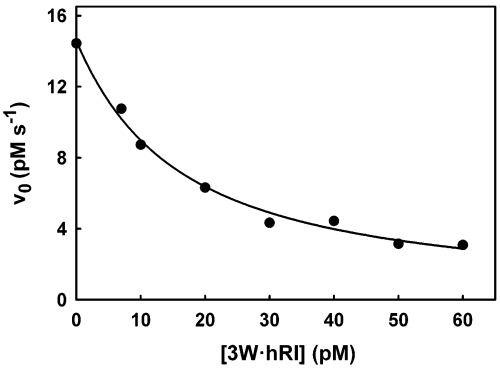

FIGURE 6: Inhibition of EDN by 3W. Data are plotted as v_0 vs [I], with conditions as described in Experimental Procedures. The curve fit was calculated with an equation for tight-binding inhibition (*23*, *60*).

method would be feasible. Additional assays were then conducted with 15−30 pM inhibitor. The K_i values obtained were 1.5 pM (Y434A/D435A) and 0.8 pM (Y434A/Y437A). These are 540- and 290-fold higher, respectively, than for the wild-type complex and 21- and 120-fold, respectively, beyond those expected if the mutational effects were independent and additive. The magnitudes of these superadditivities ($\Delta\Delta\Delta G$ values) are 1.8 kcal/mol (Y434A/D435A) and 2.8 kcal/mol (Y434A/Y437A). For the 434/435 variant, the superadditivity reflects only the dissociation process (k_d values are calculated as K_i times k_a; Table 3). For the 434/437 variant, however, effects on both k_a and k_d are superadditive.

The increase in K_i for the complex of Ang with 3W (6300-fold; ref *23*) is not as large as with Y434A/D435A and Y434A/Y437A, and we therefore attempted to determine k_d for the EDN complex by the standard method. Although Ang was an efficient scavenger, dissociation was too rapid for accurate measurement. The k_d value was estimated to be $> 1 \times 10^{-3}$ s^{-1}, suggesting that K_i is well into the range that can be determined from a plot of v_0 vs [I]. From the measured k_a value, 1.1×10^8 M^{-1} s^{-1}, preincubations of 20 min were calculated to be sufficient to reach steady-state for v_0 assays at the 3W concentrations to be used (Figure 6). The K_i value obtained was 13 pM. This value is almost 5000-fold above that for the wild-type complex and signifies a large degree of superadditivity of mutational effects ($\Delta\Delta\Delta G = -2.5$ kcal/mol).

DISCUSSION

The complexes of RI with its most avid ligands (Ang, EDN, and RNase 4; $K_i = 0.7-4$ fM, refs *4*, *10*, and *11*) are among the tightest protein−protein interactions on record, to our knowledge rivaled only by the complexes of colicin E9 with its immunity protein Im9 (0.09 fM at low ionic strength, ref *46*), TIMP-2 with gelatinase A (0.6 fM, ref *47*), and ecotin with chymotrypsin (4 fM, ref *48*). In achieving the high affinity of RI for multiple targets, nature had to solve a molecular recognition problem opposite from that most commonly faced. For the vast majority of proteins that strongly associate with other proteins, proper functioning requires that the correct binding partner can be effectively distinguished from numerous structural homologues (e.g., ref *49*) (i.e., tight binding and stringent selectivity must coevolve). For the RI−RNase system, however, a key requirement during the evolution of high affinity binding has been to maintain very relaxed selectivity, so that the inhibitor can protect cells from all of the pancreatic RNase superfamily enzymes it might encounter. This is not a straightforward task. The RNases themselves have evolved to carry out widely divergent functions (*9*) and contain few potential points of attachment that are well-conserved throughout (*50*). Indeed, the enzymatic active site itself, which is the actual functional target of RI, is structurally invariant only at its catalytic center, the P_1 subsite.[2]

How has nature solved this problem? Previous studies have provided a fairly clear, albeit still incomplete, picture of how

[2] The active sites of RNase A and its homologues contain multiple subsites P_n, B_n, and R_n for binding the phosphate, nucleobase, and ribose components of RNA substrates, respectively (*1*). The core subsites are P_1, where phosphodiester bond cleavage occurs; B_1, which binds the pyrimidine whose associated ribose contributes its 3′ oxygen to the phosphate in P_1; and B_2, which binds the base of the nucleotide that provides the 5′ oxygen to the scissile bond.

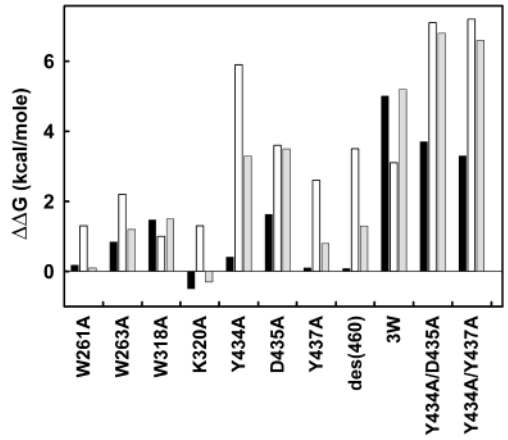

FIGURE 7: Comparison of $\Delta\Delta G$ values for single and multisite replacements in hRI complexes with EDN (black bars), RNase A (open bars), and Ang (gray bars). The values for RNase A and Ang complexes are from earlier studies (*2*, *22*, *23*).

RI recognizes two of its ligands, Ang and RNase A (K_i = 0.7 and 44 fM, respectively, refs *10* and *34*). The crystal structures of the pRI·RNase A (*19*, *20*) and hRI·Ang (*21*) complexes reveal large interfaces (Figure 1), containing 26−28 residues on RI and 24 on each ligand. Although nearly two-thirds of the contact residues on RI are the same in the two complexes, only a relatively small number of the specific interactions correspond. This suggests either that the few shared interactions are energetically dominant or that tight binding to RNase A and Ang is achieved through largely different contacts. The results of extensive mutational studies (*2*, *22*, *23*, *31*, *51*−*54*) examining most of the hRI residues that contact RNase A and Ang, as well as many residues on the ligands, support the latter mechanism.

Individual replacements or deletions of four hRI residues (Tyr434, Asp435, Tyr437, and Ser460) that contact the active site of RNase A produce $\Delta\Delta G$ values of 2.6−5.9 kcal/mol. Although all of these mutations also diminish affinity for Ang, the effect is comparable only for the substitution of Asp435 by Ala (Table 1, Figure 7) (*2*). Asp435 forms two hydrogen bonds with the critical catalytic residue Lys40 in the hRI·Ang crystal structure and is thought to form analogous interactions in the RNase A complex (*20*, *21*)[3]. The contacts of Tyr434, Tyr437, and Ser460 with RNase A and Ang correspond less well. In the Ang complex, another residue from this region of RI, Trp438 (main-chain O), forms energetically important hydrogen bonds with the P_2 site residue Arg5 (*31*); these interactions are not replicated in the RNase A complex, where Arg5 is substituted by Ala.

hRI also makes numerous contacts with the $\beta4/\beta5$ loop of RNase A and Ang (residues 86−93 and 84−93, respectively) far from the enzymatic active site. The structure of this loop is quite different in the two proteins. Consequently, although many of the same hRI residues are contacted (those in the 206−375 segment; Figure 1), there is no correspondence between the interactions formed, and the effects of most single-site replacements differ greatly (*23*). Seven substitutions decrease the binding energy for the RNase A complex by >1 kcal/mol, versus three for the Ang complex. Other parts of the interfaces, containing less concentrated groups of contact residues, appear to provide only a small portion of the binding energy (*23*, *31*).

Another important difference between the hRI·RNase A and the hRI·Ang complexes concerns the functional connectivities between various interface components. The sum of $\Delta\Delta G$ values for all single-residue replacements on hRI in the RNase A complex vastly exceeds ΔG for the complex. Thus, the combined effects of the mutations is subadditive, signaling the presence of positive cooperativity. So far, multisite mutagenesis has revealed three specific instances of strong subadditivity (*22*, *23*). In contrast, the sum of $\Delta\Delta G$ values for replacements in the Ang complex is well below ΔG (i.e., the mutational effects are superadditve, signaling negative cooperativity). Numerous examples of this were found by examination of complexes that contained two or three hRI and/or Ang mutations (*22*, *23*). Taking these cooperativities into account, it was concluded (*23*) that about two-thirds of the binding energy for the Ang complex derives from interactions of the C-terminal hRI and the enzymatic active site, with most of the remainder provided by the interactions of four hRI Trps (261, 263, 318, and 375) and the $\beta4/\beta5$ loop of Ang. The RNase A complex contains the same primary hot spot, although as noted its detailed functioning differs considerably, and in this case the remainder of the binding energy seems to be distributed among many interactions outside the hot spot.

In light of these findings, it seemed likely that RI might achieve tight binding of all of its ligands largely through interactions of its C-terminal region with the enzymatic active site. The catalytic Lys appeared to be an especially good candidate for a universal anchoring residue. Its side chain adopts similar positions in all ligands whose structures have been determined (*1*, *14*, *16*, *18*, *55*-*57*) and might be expected to form strong hydrogen bonds with RI Asp435 in all cases. RI displays considerable adaptability in forming additional tight interactions with the variable regions of the active sites of RNase A and Ang beyond P_1, and it seemed likely that this would extend to recognition of other ligands as well.

Contrary to this hypothesis, we find that Ala substitutions of hRI residues Tyr434, Asp435, and Tyr437, and deletion of Ser460 have no major effect on affinity for EDN (Table 1, Figure 7). Even the replacement of Asp435 produces a $\Delta\Delta G$ value of only 1.5 kcal/mol, less than half of that measured with RNase A and Ang. The disparities for the other variants (which give $\Delta\Delta G$ values $\leq$0.4 kcal/mol) are even larger. Modeling of the RI·EDN complex suggests some possible reasons for the small magnitudes of the changes produced by 434, 437, and 460 mutations. The hydrogen bond of Asp435 with Lys38 seen in the initial superposition models is no longer present after energy minimization, reflecting a ~1 Å shift in the position of the 435 carboxylate. This movement may be a consequence of the need to resolve structural clashes involving other residues, and it is conceivable that it also occurs during formation of the actual complex. Much of the energy contributed by Tyr434 to binding of RNase A and Ang appears to derive from the hydrophobic burial of this residue against the ligand, including the alkyl portion of Lys40/41. In the energy-minimized RI·EDN model complexes, access of Tyr434 to this precise region is impeded by Gln34 (which has no

[3] These interactions are not observed in the pRI·RNase A crystal structure, where a sulfate ion from the crystallization medium binds the corresponding lysine of RNase A. However, they most likely occur under the conditions of the kinetic determinations, where no sulfate is present (*2*).

structural analogue in RNase A or Ang). The RI·EDN models also suggest that Tyr437 of RI is not well-positioned to form strong interactions, as it does with the B_2 purine binding subsite in RNase A (*20*). For Ser460, the models reveal no contacts comparable to the hydrogen bonds with Lys7 and His8 in the RNase A and Ang complexes, respectively.

The RI·EDN models identified nine hRI residues outside this region as potentially important contacts for EDN. Nonetheless, individual replacements of only two of these residues (Trp263 and Trp318) diminished affinity significantly, and in neither case was the decrease large ($\Delta\Delta G$ = 0.9 and 1.5 kcal/mol, respectively) (Table 2). The effects of four of the replacements (Trp261, Trp263, Trp318, and Lys320 to Ala) on binding to RNase A and Ang were measured previously (*23*) (Figure 7). In all but one instance (Trp318 to Ala), $\Delta\Delta G$ values were much larger for the RNase A than the EDN complex. In contrast, the changes for the Ang complex were indistinguishable from those with EDN. Despite this, the specific interactions with the two ligands must be entirely different because the contacts for these hRI residues on Ang, which lie on the $\alpha 2/\beta 1$ and $\beta 4/\beta 5$ loops, are not conserved in EDN.

The sum of the (positive) $\Delta\Delta G$ values for the 13 single-residue hRI mutations investigated here (Tables 1 and 2) is only 4.8 kcal/mol (i.e., 24% of the binding energy for the wild-type hRI·EDN complex). Our findings with multi-residue hRI variants (Table 3) indicate that some of this shortfall is due to negative cooperativity. The $\Delta\Delta G$ values for replacements of Tyr434 together with either Asp435 or Tyr437 (3.3 and 3.7 kcal/mol, respectively) are well beyond the sums for the individual mutations (Tables 1 and 3). $\Delta\Delta G$ for the combination of W261A, W263A, and W318A is even larger (5.0 kcal/mol) and again greatly exceeds the sum for the separate replacements (Tables 2 and 3). Possible physical bases for superadditivities of mutational effects in the hRI·Ang complex were discussed previously (*22*, *23*) and may apply to the EDN complex as well. In general, superadditivity can occur if replacement of one residue within a group strengthens the contacts of other residues or if the loss of the interactions of one residue allows the formation of new, compensatory interactions by other group members (*48*). The subadditivity of these same groups of replacements in the RNase A complex (*22*, *23*) argues strongly against an alternative explanation (i.e., that the accumulation of replacements causes significant perturbations in hRI structure that disrupt interactions of other residues).

The results obtained with multisite variants suggest that interactions of the Trp-rich region of RI provide a considerable amount of the energy for binding EDN, similar to that for binding Ang (Figure 7). The C-terminal hot spot for binding RNase A and Ang, despite the initial impression gleaned from single-site mutagenesis, also plays an important role in recognition of EDN. However, the magnitude of its contribution seems unlikely to approach that made in the RNase A and Ang complexes, even if some additional negative cooperativities in its functioning remain to be uncovered. This would then imply that some of the RI residues that are critical for high affinity binding of EDN have not yet been examined, although no such residues were evident from the modeled complexes. In this regard, some specific limitations of modeling the RI·EDN complex should be noted. The distance between the N- and C-terminal ends of the RI horseshoe in the two models might differ appreciably from that in the actual complex; this opening appears to be highly ligand-dependent (*20*, *21*) and probably would not have been adjusted adequately during energy minimization. (Despite this malleability, a model of the RI·Ang complex generated by similar procedures from the RNase A complex crystal structure predicted reasonably well how the proteins fit together, ref *20*.) Compositional differences between the recombinant EDN whose crystal structure was used for modeling and the natural protein used in our study must also be considered. (i) The recombinant material is extended at its N-terminus by a Met residue, which intrudes into the contact region in the models. (ii) Natural EDN, unlike the recombinant protein, is N-glycosylated at five sites (*43*), two of which (Asn65 and Asn84) are not far from the contact surface in the models. (iii) In natural EDN, Trp7 is C-mannosylated (*58*). This residue is in close proximity to RI in the models, and an added mannose group would clash with the main chain of Glu440.

A more complete understanding of the physical basis for high-affinity binding of EDN by RI will require the determination of a three-dimensional structure for the complex as well as additional mutational studies, including a complementary analysis of the effects of replacements in EDN. As the investigations of the RI complexes with RNase A, Ang, and now EDN have made clear, it will be particularly important to dissect cooperative features of the interface. Indeed, it seems likely that the detailed functioning of protein−protein complexes in general cannot be delineated without focusing attention on this underappreciated aspect.

ACKNOWLEDGMENT

We thank Matthew Crawford for excellent technical assistance, Dr. Evangelia Chrysina for assistance with the modeling of the RI·EDN complexes, Shalini Iyer for preparing Figure 1, and Drs. James F. Riordan and Kapil Kumar for helpful discussions.

REFERENCES

1. Richards, F. M., and Wyckoff, H. W. (1973) in *The Atlas of Molecular Structures in Biology* (Phillips, D. C., and Richards, F. M., Eds.), Clarendon Press, Oxford.
2. Chen, C. Z., and Shapiro, R. (1997) *Proc. Natl. Acad. Sci. U.S.A. 94*, 1761−1766.
3. Lee, F. S., and Vallee, B. L. (1993) *Prog. Nucleic Acid Res. Mol. Biol. 44*, 1−30.
4. Hofsteenge, J. (1997) in *Ribonucleases. Structures and Functions* (D'Alessio, G., and Riordan, J. F., Eds.) pp 621−658, Academic Press, New York.
5. Shapiro, R. (2001) *Methods Enzymol. 341*, 611−628.
6. Beintema, J. J., Schuller, C., Irie, M., and Carsana, A. (1988) *Prog. Biophys. Mol. Biol. 51*, 165−192.
7. Leland, P. A., Schultz, L. W., Kim, B. M., and Raines, R. T. (1998) *Proc. Natl. Acad. Sci. U.S.A. 95*, 10407−10412.
8. Shapiro, R., and Vallee, B. L. (1987) *Proc. Natl. Acad. Sci. U.S.A. 84*, 2238−2241.
9. D'Alessio, G., and Riordan, J. F., Eds. (1997) *Ribonucleases: Structures and Functions*, Academic Press, New York.
10. Lee, F. S., Shapiro, R., and Vallee, B. L. (1989) *Biochemistry 28*, 225−230.
11. Shapiro, R., and Vallee, B. L. (1991) *Biochemistry 30*, 2246−2255.
12. Boix, E., Wu, Y., Vasandani, V. M., Saxena, S. K., Ardelt, W., Ladner, J., and Youle, R. J. (1996) *J. Mol. Biol. 257*, 992−1007.

13. Beintema, J. J., Breukelman, H. J., Carsana, A., and Furia, A. (1997) in *Ribonucleases: Structures and Functions* (D'Alessio, G., and Riordan, J. F., Eds.) pp 245−269, Academic Press, New York.
14. Wlodawer, A., Svensson, L. A., Sjolin, L., and Gilliland, G. L. (1988) *Biochemistry 27*, 2705−2717.
15. Acharya, K. R., Shapiro, R., Allen, S. C., Riordan, J. F., and Vallee, B. L. (1994) *Proc. Natl. Acad. Sci. U.S.A. 91*, 2915−2919.
16. Mosimann, S. C., Newton, D. L., Youle, R. J., and James, M. N. (1996) *J. Mol. Biol. 260*, 540−552.
17. Leonidas, D. D., Boix, E., Prill, R., Suzuki, M., Turton, R., Minson, K., Swaminathan, G. J., Youle, R. J., and Acharya, K. R. (2001) *J. Biol. Chem. 276*, 15009−15017.
18. Terzyan, S. S., Peracaula, R., de Llorens, R., Tsushima, Y., Yamada, H., Seno, M., Gomis-Ruth, F. X., and Coll, M. (1999) *J. Mol. Biol. 285*, 205−214.
19. Kobe, B., and Deisenhofer, J. (1995) *Nature 374*, 183−186.
20. Kobe, B., and Deisenhofer, J. (1996) *J. Mol. Biol. 264*, 1028−1043.
21. Papageorgiou, A. C., Shapiro, R., and Acharya, K. R. (1997) *EMBO J. 16*, 5162−5177.
22. Chen, C. Z., and Shapiro, R. (1999) *Biochemistry 38*, 9273−9285.
23. Shapiro, R., Ruiz-Gutierrez, M., and Chen, C. Z. (2000) *J. Mol. Biol. 302*, 497−519.
24. Clackson, T., and Wells, J. A. (1995) *Science 267*, 383−386.
25. Ackerman, S. J., Loegering, D. A., Venge, P., Olsson, I., Harley, J. B., Fauci, A. S., and Gleich, G. J. (1983) *J. Immunol. 131*, 2977−2982.
26. Iwama, M., Kunihiro, M., Ohgi, K., and Irie, M. (1981) *J. Biochem. (Tokyo) 89*, 1005−1016.
27. Sorrentino, S., Glitz, D. G., Hamann, K. J., Loegering, D. A., Checkel, J. L., and Gleich, G. J. (1992) *J. Biol. Chem. 267*, 14859−14865.
28. Rosenberg, H. F., and Domachowske, J. B. (2001) *Methods Enzymol. 341*, 273−286.
29. Polakowski, I. J., Lewis, M. K., Muthukkaruppan, V. R., Erdman, B., Kubai, L., and Auerbach, R. (1993) *Am. J. Pathol. 143*, 507−517.
30. Snyder, M. R., and Gleich, G. J. (1997) in *Ribonucleases: Structures and Functions* (D'Alessio, G., and Riordan, J. F., Eds.) pp 425−444, Academic Press, New York.
31. Shapiro, R., and Vallee, B. L. (1992) *Biochemistry 31*, 12477−12485.
32. Lee, F. S., and Vallee, B. L. (1990) *Biochemistry 29*, 6633−6638.
33. Russo, N., and Shapiro, R. (1999) *J. Biol. Chem. 274*, 14902−14908.
34. Lee, F. S., Auld, D. S., and Vallee, B. L. (1989) *Biochemistry 28*, 219−224.
35. Ho, S. N., Hunt, H. D., Horton, R. M., Pullen, J. K., and Pease, L. R. (1989) *Gene 77*, 51−59.
36. Kelemen, B. R., Klink, T. A., Behlke, M. A., Eubanks, S. R., Leland, P. A., and Raines, R. T. (1999) *Nucleic Acids Res. 27*, 3696−3701.
37. Kao, R. Y., Jenkins, J. L., Olson, K. A., Key, M. E., Fett, J. W., and Shapiro, R. (2002) *Proc. Natl. Acad. Sci. U.S.A. 99*, 10066−10071.
38. Cha, S. (1975) *Biochem. Pharmacol. 24*, 2177−2185.
39. Vicentini, A. M., Kieffer, B., Matthies, R., Meyhack, B., Hemmings, B. A., Stone, S. R., and Hofsteenge, J. (1990) *Biochemistry 29*, 8827−8834.
40. Stuart, D. I., Levine, M., Muirhead, H., and Stammers, D. K. (1979) *J. Mol. Biol. 134*, 109−142.
41. Brunger, A. T., Adams, P. D., Clore, G. M., DeLano, W. L., Gros, P., Grosse-Kunstleve, R. W., Jiang, J. S., Kuszewski, J., Nilges, M., Pannu, N. S., Read, R. J., Rice, L. M., Simonson, T., and Warren, G. L. (1998) *Acta Crystallogr. D54*, 905−921.
42. Rice, L. M., and Brunger, A. T. (1994) *Proteins 19*, 277−290.
43. Beintema, J. J., Hofsteenge, J., Iwama, M., Morita, T., Ohgi, K., Irie, M., Sugiyama, R. H., Schieven, G. L., Dekker, C. A., and Glitz, D. G. (1988) *Biochemistry 27*, 4530−4538.
44. Hofsteenge, J., Kieffer, B., Matthies, R., Hemmings, B. A., and Stone, S. R. (1988) *Biochemistry 27*, 8537−8544.
45. Lee, F. S., Fox, E. A., Zhou, H. M., Strydom, D. J., and Vallee, B. L. (1988) *Biochemistry 27*, 8545−8553.
46. Wallis, R., Moore, G. R., James, R., and Kleanthous, C. (1995) *Biochemistry 34*, 13743−13750.
47. Hutton, M., Willenbrock, F., Brocklehurst, K., and Murphy, G. (1998) *Biochemistry 37*, 10094−10098.
48. Eggers, C. T., Wang, S. X., Fletterick, R. J., and Craik, C. S. (2001) *J. Mol. Biol. 308*, 975−91.
49. Kleanthous, C., Hemmings, A. M., Moore, G. R., and James, R. (1998) *Mol. Microbiol. 28*, 227−233.
50. Shapiro, R., Riordan, J. F., and Vallee, B. L. (1995) *Nat. Struct. Biol. 2*, 350−354.
51. Lee, F. S., and Vallee, B. L. (1989) *Biochemistry 28*, 3556−3561.
52. Shapiro, R., and Vallee, B. L. (1989) *Biochemistry 28*, 7401−7408.
53. Neumann, U., and Hofsteenge, J. (1994) *Protein Sci. 3*, 248−256.
54. Haigis, M. C., Kurten, E. L., Abel, R. L., and Raines, R. T. (2002) *J. Biol. Chem. 277*, 11576−81.
55. Leonidas, D. D., Shapiro, R., Allen, S. C., Subbarao, G. V., Veluraja, K., and Acharya, K. R. (1999) *J. Mol. Biol. 285*, 1209−1233.
56. Swaminathan, G. J., Holloway, D. E., Veluraja, K., and Acharya, K. R. (2002) *Biochemistry 41*, 3341−3352.
57. Boix, E., Leonidas, D. D., Nikolovski, Z., Nogues, M. V., Cuchillo, C. M., and Acharya, K. R. (1999) *Biochemistry 38*, 16794−16801.
58. Loffler, A., Doucey, M. A., Jansson, A. M., Muller, D. R., de Beer, T., Hess, D., Meldal, M., Richter, W. J., Vliegenthart, J. F., and Hofsteenge, J. (1996) *Biochemistry 35*, 12005−12014.
59. Kraulis, P. J. (1991) *J. Appl. Crystallogr. 24*, 946−950.
60. Morrison, J. F. (1969) *Biochim. Biophys. Acta 185*, 269−286.

BI026852O